



Coprecipitation synthesis of transition metal (Al, Mn, Cu, Ag) doped zinc oxide nanopowders: characterization, photocatalytic test, and comparison study

Rabie Amari^{1,2} · Abdelhamid Guellil³ · Smail Terchi^{1,4} · Bahri Deghfel^{1,5} · Abdelhalim Zoukel⁶ · Djamel Allali⁷ · Elhadj Benrezgua^{1,8} · Ammar Boukhari^{1,9} · Ahmad Azmin Mohamad¹⁰

Received: 26 May 2023 / Revised: 26 October 2023 / Accepted: 9 November 2023 / Published online: 24 November 2023

© The Author(s) under exclusive licence to Australian Ceramic Society 2023

Abstract

The study successfully produced ZnO and ZnO nanoparticles doped with transition metals (TMZO-NPs) using the coprecipitation method. Various properties of these nanoparticles were examined, including their structure, morphology, electronic behavior, optical characteristics, vibrations, and photocatalytic abilities. The analysis confirmed that all nanoparticles possessed a hexagonal wurtzite crystalline structure, with particle size being influenced by the presence of transition metals (Al, Ag, Cu, Mn). The particles exhibited a preference for orientation along the (002) axis. The shift in peak positions towards higher angles suggested that the TM might replace Zn ions in the ZnO lattice. The surface structure of the nanoparticles displayed a combination of spherical and hexagonal shapes. Further analysis identified important bands related to the stretching modes of TM–O and Zn–O bonds. The absorption properties and edges were also affected by the presence of TM. In the degradation study, both pure ZnO and TMZO-NPs were tested for their ability to break down methylene blue (MB) under UV light exposure for 90 min. Among the nanoparticles, Al-doped ZnO (AlZO-NPs) demonstrated the highest degradation efficiency, achieving 97.14% removal of MB within the given exposure time. The photocatalytic process followed a pseudo-first-order kinetics, indicating a strong correlation. This suggests that AlZO-NPs hold promise as a material for use in photocatalytic applications.

Keywords Transition metal · Zinc oxide · Nanopowder · Co-precipitation · Photocatalysis

✉ Bahri Deghfel
b_deghfel@yahoo.fr; bahri.deghfel@univ-msila.dz

✉ Ahmad Azmin Mohamad
aam@usm.my

¹ Laboratory of Materials and Renewable Energy, Faculty of Sciences, University of M'sila, 28000 M'sila, Algeria

² Department of Civil Engineering, Faculty of Technology, University of M'sila, 28000, M'sila, Algeria

³ Department of Chemistry, Faculty of Sciences, University of Biskra, 7000 Biskra, Algeria

⁴ Department of Chemistry, Faculty of Sciences, University of M'sila, 28000 M'sila, Algeria

⁵ Department of Physics, Faculty of Sciences, University of M'sila, 28000 M'sila, Algeria

⁶ Laboratory Physico-Chemistry of Materials, University of Laghouat, 3000 Laghouat, Algeria

⁷ Physics and Chemistry of Materials Lab, Faculty of Sciences, University of M'sila, 28000 M'sila, Algeria

⁸ Department of Natural and Life Sciences, Faculty of Sciences, University of M'sila, 28000 M'sila, Algeria

⁹ Department of Mechanical Engineering, Faculty of Technology, University of M'sila, 28000 M'sila, Algeria

¹⁰ Energy Materials Research Group (EMRG), School of Materials and Mineral Resources Engineering, Universiti Sains Malaysia, 14300 Nibong Tebal, Pulau Pinang, Malaysia

Introduction

ZnO wurtzite structure is the most stable phase at ambient temperature. It exhibits high transparency, high exciton binding energy, and a large direct band gap [1–10]. During the past years, many studies have been reported on TMZO-NPs [3–21]. In addition to the preparation conditions and synthesis methods [20], the doping process by TM allows ZnO to exhibit the desired properties [22]. These are essential requirements for several applications, such as photocatalysis [23], transparent conducting electrodes [24], gas sensors, and light-emitting diodes [25].

The dopant can exist as substitutional or interstitial sites in the host lattice creating mixed or localized states at the edges or the middle of the forbidden band, which narrow the band-gap of the oxide, enhance its visible light activity and increase the photogenerated electrons and holes. It can create trapping states, which prevent the rapid charge recombination [26].

Many workers have shown a growing interest in elaborating ZnO-NPs using a simple and low-cost process such as co-precipitation [3, 6, 9, 27]. Higher crystallinity, smaller particle size, higher specific surface area, and higher average pore diameter are among the numerous attractive properties of NPs elaborated by the co-precipitation route [27]. Since TMZO-NPS is widely used for photocatalytic applications, many works on these NPs have been published in the past years [3, 6, 8, 9, 28]. However, works on the effect of doping of various TM in ZnO on the photocatalytic test to remove dyes from water are still limited. Hence, taking up a work focused mainly on the properties of ZnO NPs doped with a specified TM element (Al, Mn, Cu, and Ag) and prepared by co-precipitation technique is of interest.

Due to the various textile industry processes, dyes enter the environment [7]. Among these dyes, MB is now used in this industry. The pollutants are treated using osmosis, coagulation, ultrafiltration, and photodegradation techniques. It is later becoming an effective, inexpensive, and environmentally friendly technology, utilizing appropriate light sources and having the potential for worldwide application. Several attempts have been made to prepare the materials for photodegradation [6, 7, 9]. Other than that, the high mechanical stress tolerance and compatibility with other organic compounds of various metal oxides are well recognized [29–31]. ZnO can be considered a valid photocatalyst due to several factors, including its appropriate band gap, high absorption coefficient, large exciton binding energy, and sufficient electron mobility [7, 32, 33].

The photocatalytic performance of the catalyst relies significantly on its optical properties, crystalline structure, surface chemistry, and electronic characteristics. Nevertheless, significant challenges, such as the rapid recombination of photogenerated electron–hole pairs, the low surface chemistry and the mismatch of bandgap of metal oxides and light spectrum, limit the photocatalytic applications. Although metal oxides have shown successful utility as photocatalysts, addressing the

aforementioned limitations often involves implementing various strategies, including metal doping and morphology tailoring [26, 34].

In the present work, ZnO and TMZO-NPs, at concentration $x=3.12$, were elaborated by co-precipitation route. The properties of TMZO-NPs, such as morphological, structural, optical, electronic, and vibrational properties, were investigated. Apart from that, degradation by pure ZnO and TMZO-NPs of the MB was tested after 90 min UV light exposure.

Experimental

ZnO and TMZO-NPs at content $x=3.12\%$ were prepared by the co-precipitation process. Zinc acetate dihydrate [$\text{Zn}(\text{CH}_3\text{COO})_2 \cdot 2\text{H}_2\text{O}$; $\geq 99.0\%$], manganese acetate dihydrate [$\text{Mn}(\text{CH}_3\text{COO})_2 \cdot 2\text{H}_2\text{O}$; 97.0%], silver nitrate [AgNO_3 ; $\geq 99.0\%$], copper (II) nitrate trihydrate [$\text{Cu}(\text{NO}_3)_2 \cdot 3\text{H}_2\text{O}$; 99.9%], and aluminum chloride hexahydrate [$\text{AlCl}_3 \cdot 6\text{H}_2\text{O}$; 99.0%] were used as precursors. All chemical reagents were purchased from Sigma-Aldrich. Here, zinc acetate dihydrate was dissolved in 200 ml of distilled water and stirred continuously for 1 h by a magnetic stirrer at 60°C . Stoichiometric amounts of TM precursor were also dissolved in the solution for the case of TMZO-NPs. Distilled water was used to dissolve sodium hydroxide (NaOH), which was then added drop-wise to raise the pH of the solution to ~ 9 [35]. Subsequently, a precipitate appears after stirring for 1 h at 60°C . The obtained product was washed several times in a centrifuge using ethanol and distilled to remove impurities. Consequently, it was dried in the oven at 150°C . The obtained samples (coarse powders) were ground into finer powders. The samples were then calcinated in a furnace at 450°C for 2 h under the air atmosphere. Figure 1 illustrates the synthesis process for all samples.

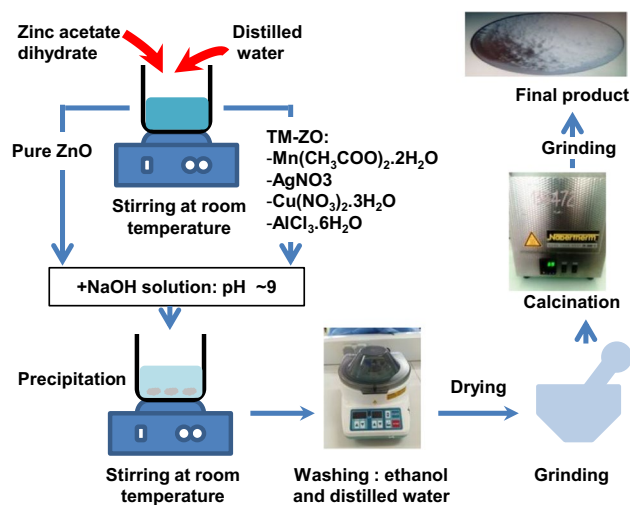


Fig. 1 Schematic synthesis of ZnO and TMZO-NPs

Pure ZnO and TMZO-NPs were determined in a 2θ range of 20° – 80° at room temperature using X-ray diffractometer XRD (XRD, X'Pert PRO MPD, with Cu- $\kappa\alpha$ radiation of $\lambda = 1.5406 \text{ \AA}$). On the other hand, scanning electron microscopy (Quattro ESEM, USA) analyzed the surface morphology. Fourier-transformed infrared spectroscopy (FTIR; Perkin-Elmer System 2000 spectrometer, USA) was conducted in the spectral range 4000 – 400 cm^{-1} . UV–Vis absorption spectroscopy (UV-3101 PC-Shimadzu, Japan), in the range of 250 – 800 nm , was used at room temperature to analyze the optical properties.

The photocatalytic performance of pure ZnO and TMZO-NPs under ambient temperature and atmosphere was performed by the degradation of MB solution (as a pollutant) irradiated by a UV lamp (30W , $\lambda > 254 \text{ nm}$) for 90 min. Note that 10 mg photocatalysts were used in 10 ml MB solution at a content of 10 mg L^{-1} . The mixtures were stirred in the dark for 30 min before the photocatalytic test to gain adsorption-deposition equilibrium. Correspondingly, the photodegradation of the MB was calculated using $(A_0 - A_t)/A_0$, where A_0 is the initial absorbance and A_t is the absorbance at a given time under exposure to UV light, both values were recorded at λ_{max} corresponding to the maximum absorbance [36]. The removal rate constant was evaluated from the slope of the plot $\ln(A_0/A_t)$ vs. irradiation time.

Results and discussions

Structural analysis

Characterization by XRD of all TMZO-NPs exhibits various diffraction peaks (Fig. 2a) whose positions match well the reported data of the ZnO reference card

(**0704–076-01**). It indicates that all TMZO-NPs are well crystallized in the wurtzite phase, and the TMZO grains prefer the orientation along the (002) axis. Moreover, no additional peaks are observed, indicating the absence of other secondary phases except for the CuZO sample. Note that a diffraction peak appears at $2\theta = 32.83^\circ$ [37].

The shift of the (002) peak position is observed for the TMZO-NPs compared to the ZnO-NPs (Fig. 2b). This shift is mainly due to the difference between the ionic radius of the TM ion (Al^{3+} ; 0.053 nm , Mn^{2+} ; 0.083 nm , Cu^{2+} ; 0.073 nm , Ag^{2+} ; 0.094 nm) and that of the Zn^{2+} (0.074 nm), leading to the difference in the lattice constants by TM doping (Table 1). A similar shift was observed in previous works [5–7, 27, 38].

The XRD data allows us to estimate the texture coefficient ($TC_{(hkl)}$) of the main peaks of pure ZnO and TMZO-NPs (Fig. 3c). Here, preferred orientations along (100), (002), and (101) planes are obvious from the $TC_{(hkl)}$ values greater than 1 for all NPs. The higher crystallinity along the (002) plane is revealed where the highest $TC_{(hkl)}$ values are observed for all prepared NPs.

The strain (ϵ), lattice constants (a and c), and average crystallite size (D) of the ZnO and TMZO-NPs are then deduced from the XRD analysis [38, 39]. Moreover, the TM doping leads to a slight variation of the parameters a while the parameters c remain approximately constant (Table 1). The obtained constants a and c are consistent with previous works [3, 8, 28, 38, 39]. Both ϵ and D , deduced from the intense (002) peak, are found to be affected by TM doping for all the samples due to the difference in the ionic radius of the TM ion compared to the Zn^{2+} [3, 8, 28, 38, 39].

Fig. 2 a XRD patterns, b (002) peak position, and c variation of $TC_{(hkl)}$ of prominent peaks for ZnO and TMZO-NPs

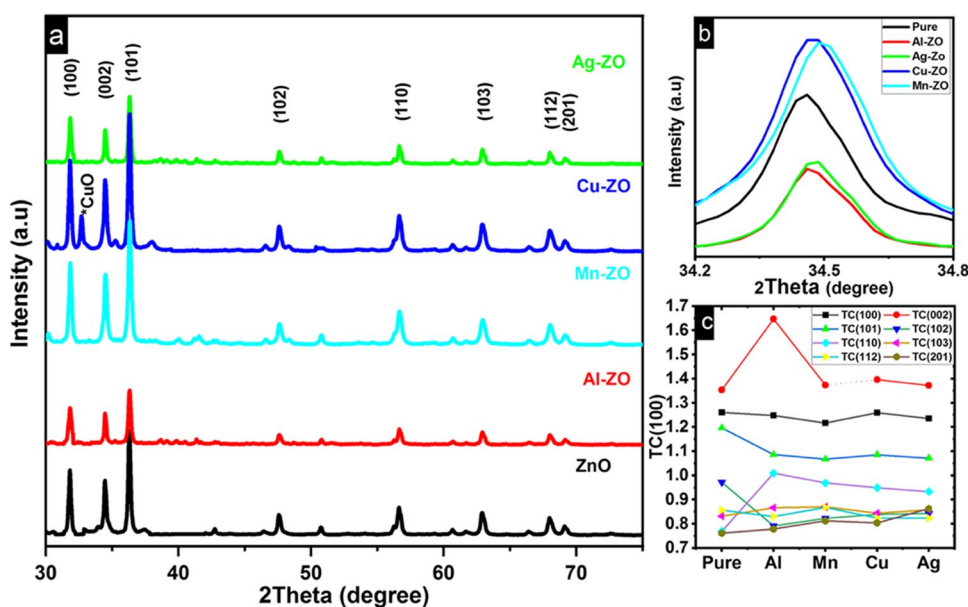
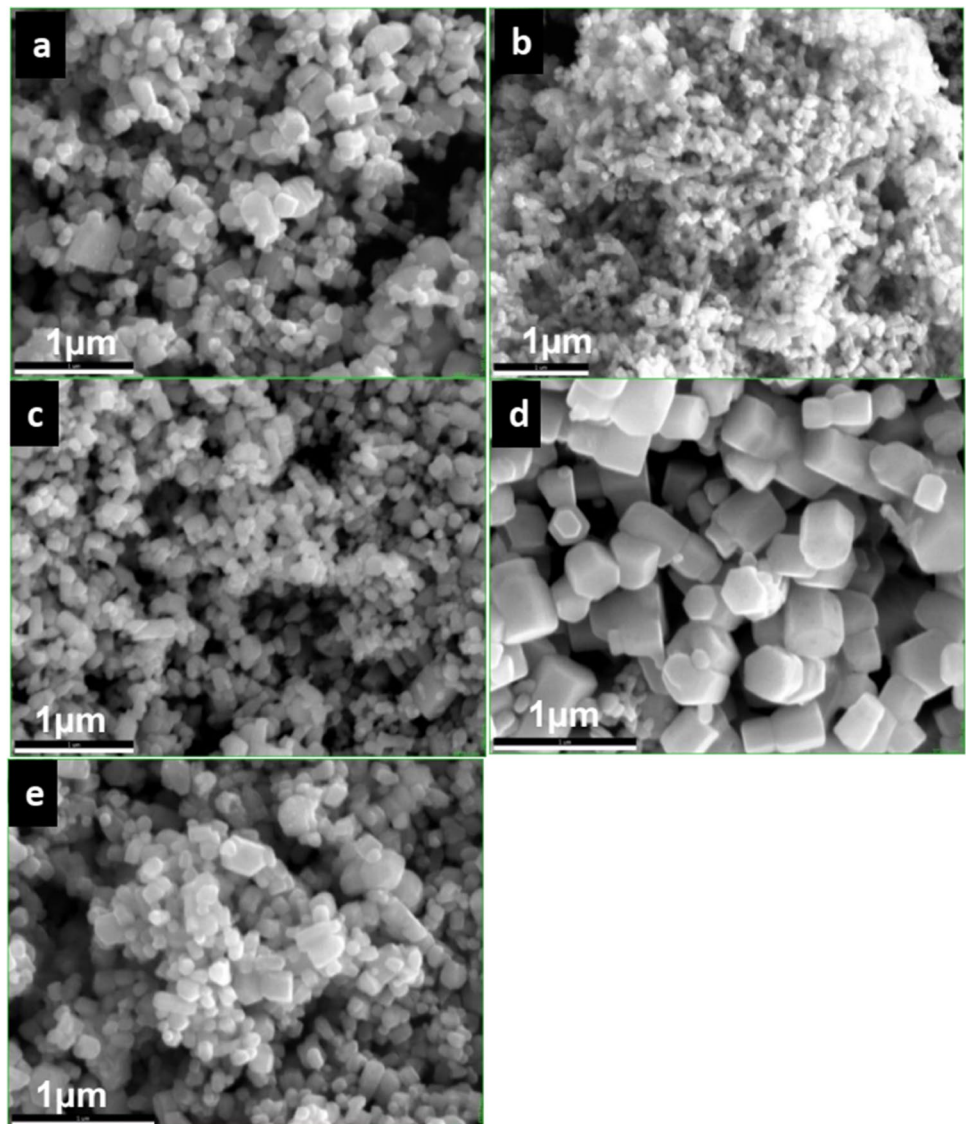


Table 1 Summary of the lattice constants ($a=b$ and c) deduced from the XRD analysis and those reported from previous works of ZnO and TMZO-NPs. Strain (ϵ) and average crystallite size (D) are also included. Here, P denotes the value from the present work

Structural parameter	ZnO	Al-ZO	Mn-ZO	Cu-ZO	Ag-ZO
$a=b$ (Å)	3.338; P	3.176; P	3.180; P	3.264; P	3.167; P
	3.241; 0%; [27]	3.242; 3%; [3]	3.245; 3%; [5]	3.275; 3.12%; [38]	3.240; 1%; [6]
	3.249; 0%; [38]	–	3.2437; 3% [10];	3.247; 3%; [40]	3.2588; 1.5%; [7]
c (Å)	5.205; P	5.203; P	5.212; P	5.209; P	5.204; P
	5.195; 0%; [27]	5.197; 3%; [3]	5.2186; 3%; [5]	5.212; 3.12% [38];	5.2066; 1%; [6]
	5.205; 0% [38];	–	5.1979; 3%; [10]	3.198; 3%; [40]	5.217; 1.5%; [7]
$\epsilon \times 10^{-2}(\%)$	21.36; P	17.97; P	16.00; P	18.82; P	19.10; P
	30.42; 0%; [27]	–	–	16.5; 3.12%; [38]	–
	19.7; 0%; [38]	–	–	16.124; 3% [8];	25.9; 1.5%; [7]
D (nm)	44.15; P	38.83; P	44.40; P	53.71; P	47.68; P
	36.61; 0%; [27]	47.42; 3%; [4]	12; 3%; [5]	20.88; 3.12%; [38]	25.66; 1%; [6]
	17.57; 0%; [38]	–	21.765; 1%; [9]	37.00; 3%; [40]	13.61; 1.5%; [7]

Fig. 3 SEM images of **a** ZnO, **b** AlZO, **c** Mn-ZO, **d** CuZO, and **e** AgZO NPs at magnifications 65 k

Morphological analysis

SEM investigates the effect of TM doping on the morphology of pure ZnO and TMZO-NPs' (Fig. 3). The surface morphology of all samples exhibits a mixture of spheroid-like and hexagon-like structures whose size is affected by TM doping, and AlZO-NPs look like the smallest ones where Al dopant prevents AlZO growth grains (Fig. 3b). This result was announced by Lee et al. [4]. CuZO NPs exhibit an interesting feature of the coexistence of spherical morphology with hexagonal structures (Fig. 3d). Due to the formation of the CuO phase and more defects, the shape and grain are larger for Cu–Zn nanoparticles than those of the other materials [41]. Hence, this result is consistent with the parameter D from XRD patterns (Table 1).

Vibrational analysis

FTIR spectroscopy is used to investigate the chemical bonding of ZnO and TMZO-NPs (Fig. 4a). The sharp bending bands of the Zn–O bond (stretching mode of Zn–O bonds) and its change due to the addition of TM into the ZnO wurtzite lattice (stretching mode of TM–O bonds) occurs at the lowest wave numbers and within the range 660–720 cm^{-1} (Fig. 4b) [8, 28, 42–45]. Note that the absorption band at 870 cm^{-1} is attributed to the C–OH group [46, 47]. Here, the absorption bands at 1060 cm^{-1} are assigned to C–N stretching vibrations. The two peaks at 1340 cm^{-1} and 1480 cm^{-1} are observed in AlZO and AgZO samples corresponding to the stretching vibrations of the C–O group [7, 43, 48]. The absorption at 1415 cm^{-1} is caused by the C=O stretching of alkanes and alkyl [8, 49].

The slight shift in the position of the bands can be assigned to the substitution of TM ion in the ZnO host lattice, which causes the change in the bond length [36, 47, 48]. It is worth noting that the variation in peak intensities and broadness are due to the unequal quantity of specific functional groups in ZnO surfaces where the reaction is varied according to the type of the dopant precursor. Here, the broad peaks in the 2800–3550 cm^{-1} band are attributed to the vibrational mode O–H bond that might come from water adsorbed on the surface [1, 50].

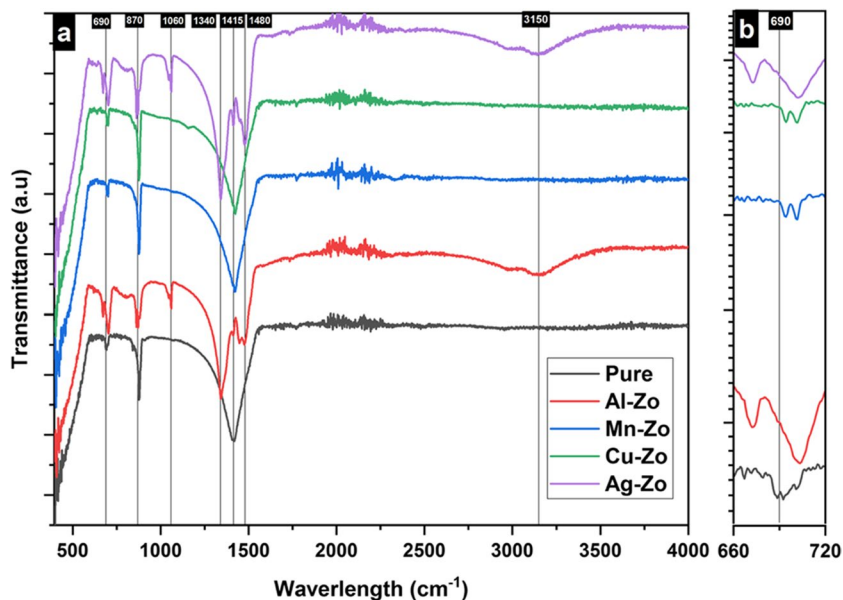
Optical analysis

UV–Vis spectroscopic analysis (λ : 300–800 nm) is conducted on pure ZnO and TMZO-NPs. Subsequently, the obtained absorbance (A) spectra (Fig. 5a) and its corresponding optical band gap (E_g) are depicted for all studied samples (Fig. 5b, c, d, e) using the Tauc equation ($(\alpha h\nu)^2 = C(h\nu - E_g)$, where $\alpha(2.303A/d)$ the absorption coefficient, ($h\nu$) is the photon energy, (d) is the film thickness, and C is a constant). Note that the absorbance is affected by the TM defects in the ZnO-NPs. The absorption edge generally shifts slightly to lower wavelengths leading to the increase E_g when heading from pure ZnO to the TMZO-NPs. Typically, these findings compare well with those reported in the literature for ZnO [3, 9, 38], AlZO [3, 4, 45], MnZO [9, 10, 51], CuZO [8, 52], and AgZO [6, 7, 53] (Table 2).

Dye removal rate

The photocatalytic performance of TMZO-NPs samples (7 mg) was performed by the degradation of 10 ml MB solution, using a UV lamp (30W, $\lambda > 254$ nm) for 90 min (Fig. 6a, c, e, g, i).

Fig. 4 a FTIR spectra and b absorption peaks within the range 660–720 cm^{-1} of pure ZnO and TMZO-NPs



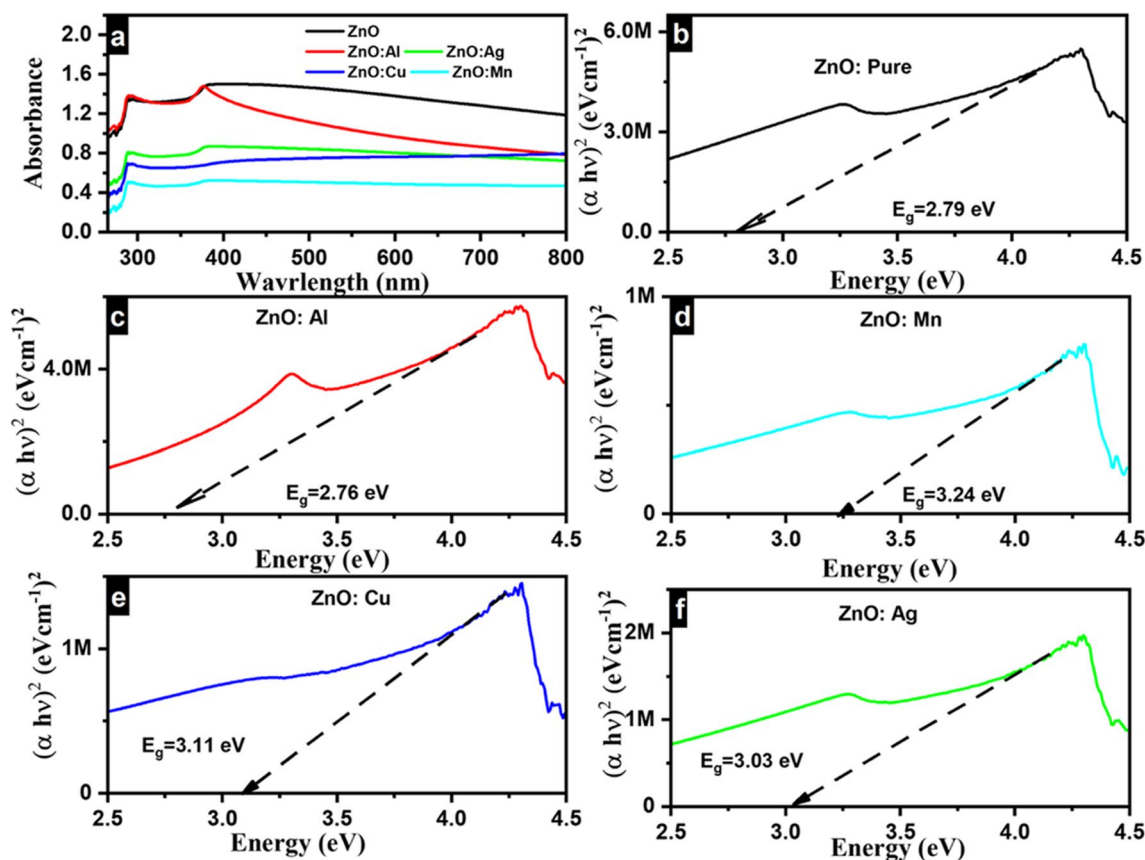


Fig. 5 a UV–Vis absorbance spectra of ZnO and TMZO-NPs. E_g of b pure ZnO, c AlZO, d MnZO, e CuZO, and f AgZO NPs

Table 2 Optical bandgap values, E_g (eV), of ZnO and TMZO-NP using the UV–Vis spectra. Other previous values are also included

Material	Present	Other
ZnO	2.79	3.34; 0%; [38]–2.91; 0%; [3]–2.79; 0%; [9]
Al-ZO	2.76	3.12; 3%; [3]–3.18; 3% [4]–3.29; 3% [45]
Mn-ZO	3.24	3.24; 1%; [9]–3.08; 3%; [10]–2.99; 4%; [51]
Cu-ZO	3.11	3.39; 3%; [8]–3.12; 2.5%; [52]–3.17; 5% [52]
Ag-ZO	3.03	3.21; 2%; [53]–3.13; 1%; [6]–2.97; 1.5%; [7]

On the other hand, Fig. 6b, d, f, h, and j illustrates the photodegradation percentage of the photocatalysts. The AlZO sample, designated by around 97.14% of MB decomposition within 90 min, exhibits the best photocatalytic activity. This finding is in accordance with the SEM results. Note that the removal rate constant of TMZO-NPs samples is derived from the linear fitting curve of the plot $\ln(A_0/A_t)$ vs. irradiation time (t) (Fig. 6b, d, f, h, j).

The linear fitting degree or the correlation coefficient (R^2 ; provides for the least square fitting to the original data) for all prepared NPs is high, except for MnZO NPs (Fig. 6b, d, f, h, j). It demonstrates the pseudo-first-order reaction

behavior for these photocatalytic processes. Apart from that, a comparative study on photocatalysis by TMZO-NPs is outlined in Table 3 [8, 28, 51, 52, 54, 55]. Despite the different methods of elaboration of NPs, photodegradation parameters estimated from this study are well compared with those reported in the literature.

Overcoming the limitations of photocatalysts is crucial for enhancing their efficiency in the photocatalytic degradation of various pollutants [26, 34, 56]. Doping with an appropriate TM can change the bandgap energy of ZnO by creating new electronic states within the forbidden band. This causes a shift in the light absorption spectrum toward visible light. It also impedes the recombination of charge carriers, leading to increased generation of super-oxides and hydroxyl radicals. The created states enable ZnO to absorb UV light and facilitate the transfer of charge from the TM-orbital to either the valence band (VB) or conduction band (VB). TM dopant acts as electron traps and slows down the recombination, thereby significantly boosting the photocatalytic performance of the TMZO-NPs compared to the ZnO-NPs. Due to the narrowing of the bandgap accompanied with the reducing of the hole-electron recombination, ALZO-NPs exhibit

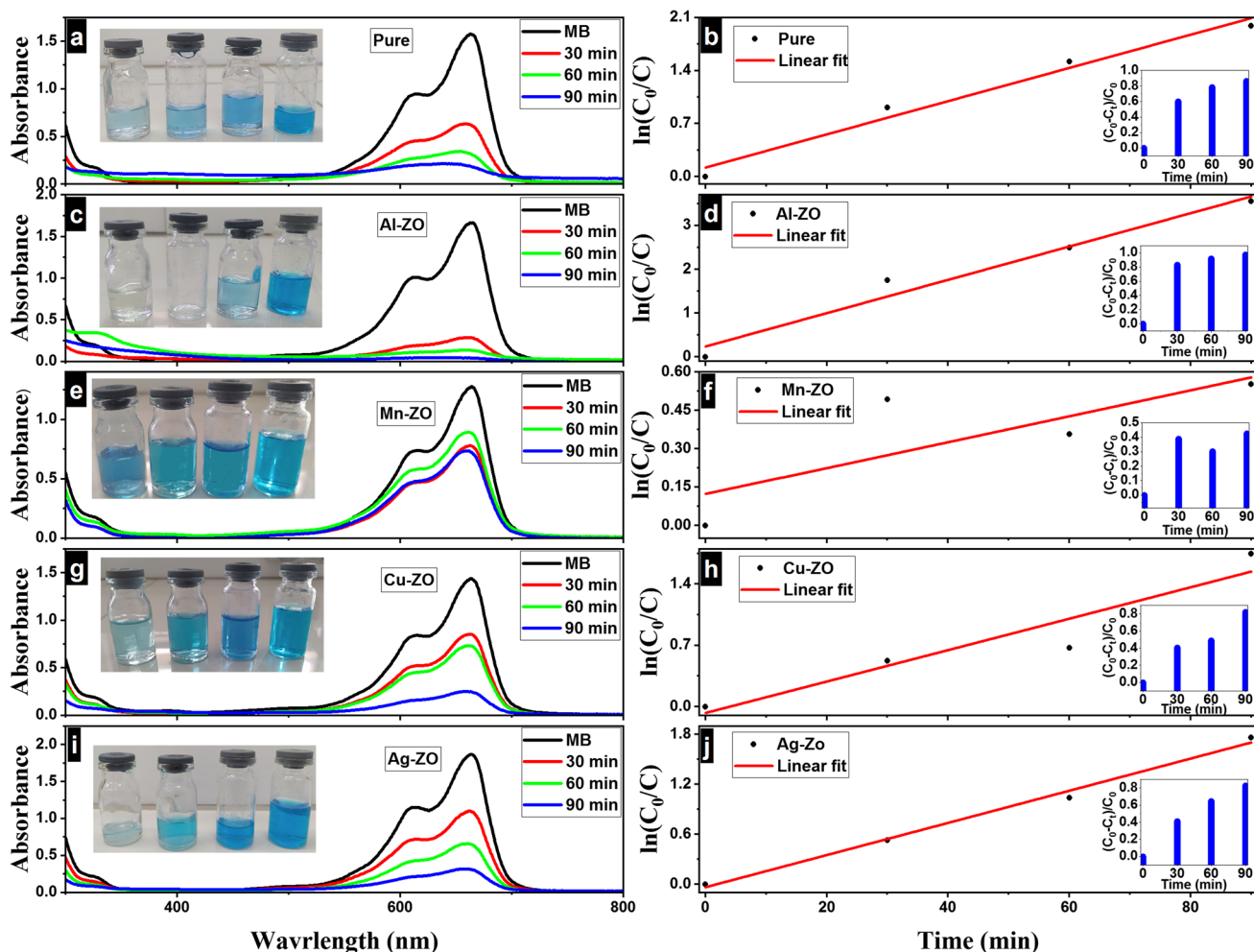


Fig. 6 Photocatalytic degradation of MB vs. time of **a** pure ZnO, **c** AlZO, **e** MnZO, **g** CuZO, and **i** AgZO NPs. Degradation percentage and removal kinetics of MB vs. time of **b** pure ZnO, **d** AlZO, **f** MnZO, **h** CuZO, and **j** AgZO NPs under UV light irradiation

Table 3 Summary of the photodegradation parameters estimated from this study and those reported from previous works of ZnO and TMZO NPs. *P* denotes values from the present work

Structural parameter	ZnO	Al-ZO	Mn-ZO	Cu-ZO	Ag-ZO
Photodegradation percentage (%)/UV irradiation time (min)	86.33%/90 min, <i>P</i> 64% /40 min; 0%; [55] 40% /180 min; 0%; [52]	97.14%/90 min, <i>P</i> 55%/180; 3%; [54] 65% /180 min; 5%; [54]	42.42%/90 min, <i>P</i> 78% /180 min; 0.5%; [28] 81% /120 min; 4%; [51]	82.50%/90 min, <i>P</i> 56.92% /90 min; 3%; [8] 81% /90 min; 2.5%; [52]	82.83%/90 min, <i>P</i> 89.5% /40 min; 2%; [55] 96.7% /40 min; 2%; [55]
Removal rate constant (s^{-1})	0.0219, <i>P</i> 0.02499; 0%; [55] 0.00246; 0%; [55]	0.0380, <i>P</i> 0.000439; 3%; [54] 0.00564; 5%; [54]	0.0051, <i>P</i> 0.0165; 0.5%; [28] –	0.0179, <i>P</i> 0.00866; 3% [8]; 0.00784; 2.5%; [52]	0.0193, <i>P</i> 0.0537; 2%; [55] 0.07496; 3%; [55]
R^2	0.9772, <i>P</i> 1.82; 0%; [55] 0.99228; 0%; [52]	0.9692, <i>P</i> 0.9978; 3%; [54] 0.9945; 5%; [54]	0.6273, <i>P</i> 0.9707; 0.5%; [28] 0.3457; 4%; [51]	0.9012, <i>P</i> – 0.99847; 2.5%; [52]	0.9929, <i>P</i> 3.92; 2%; [55] 5.47; 3%; [55]

the most pronounced photocatalytic activity compared to other synthesized NPs. Therefore, TMZO photocatalysts under UV radiation could be used as promising technology for the removal of dyes from aqueous environments through photocatalysis.

Furthermore, the grain size of ZnO-NPs is found to be affected by TM doping, and AlZO-NPs look like the smallest ones. This demonstrates the dependence of the photoactivity on the morphology and size of the photocatalyst where the AlZO-NPs exhibit the best photocatalytic activity.

Conclusions

The co-precipitation technique has been successfully used in elaborating pure ZnO and TMZO-NPs. Other than that, the structural, morphological, vibrational, and optical properties are investigated. Degradation by the elaborated NPs of the MB is also investigated under UV light. The main finding is summarized as follows:

- All NPs exhibit a hexagonal wurtzite phase with a mixture of spheroid-like and hexagon-like shaped structures and prefer orientation along the (002) axis. In contrast to the diffraction angles of the main peaks and the strain, the crystallite size exhibits a lower value by TM doping.
- Two important bands are attributed to TM-O and Zn-O stretching modes. As TM ions substitute Zn atoms in the ZnO host lattice, it induces a slight change in the bond length, leading to a small shift in the absorption peaks.
- High percentage degradation of 97.14% of the MB is achieved after 90 min of exposure under UV light irradiation for AlZO-NPs due to the small optical band gap values and the crystallite size. Note that the rate constant is increased using TMZO-NPs as catalysis, and the reaction follows pseudo-first-order kinetics with a good correlation value.

Acknowledgements B. Deghfel and S. Terchi thank the Algerian Ministry of Higher Education and Scientific Research represented by the Thematic Research Agency in Health and Life Sciences (TRAHLS) for financial support under the National Research Programs (NRP).

Declarations

Conflict of interest The authors declare no competing interests.

References

- Hessien, M., Da'na, E., Kawther, A., Khalaf, M.M.: Nano ZnO (hexagonal wurtzite) of different shapes under various conditions: fabrication and characterization. *J. Mater. Res. Exp.* **6**(8), 085057 (2019)
- Harun, K., Salleh, N.A., Deghfel, B., Yaakob, M.K., Mohamad, A.A.: DFT+ U calculations for electronic, structural, and optical properties of ZnO wurtzite structure: a review. *Results Phys.* **16**, 102829 (2020)
- Jan, T., Azmat, S., Rahman, A.U., Ilyas, S., Mehmood, A.: Experimental and DFT study of Al doped ZnO nanoparticles with enhanced antibacterial activity. *Ceram. Int.* **48**(14), 20838–20847 (2022)
- Lee, H.J., Kim, J.H., Park, S.S., Hong, S.S., Lee, G.D.: Degradation kinetics for photocatalytic reaction of methyl orange over Al-doped ZnO nanoparticles. *J. Ind. Eng. Chem.* **25**, 199–206 (2015)
- Ahmad, M., Ahmed, E., Ahmed, W., Elhissi, A., Hong, Z., Khalid, N.: Enhancing visible light responsive photocatalytic activity by decorating Mn-doped ZnO nanoparticles on graphene. *Ceram. Int.* **40**(7), 10085–10097 (2014)
- Kareem, M., Bello, I., Shittu, H., Sivaprakash, P., Adedokun, O., Arumugam, S.: Synthesis, characterization, and photocatalytic application of silver doped zinc oxide nanoparticles. *J. Clean. Mater.* **3**, 100041 (2022)
- Bhosale, A., Kadam, J., Gade, T., Sonawane, K., Garadkar, K.: Efficient photodegradation of methyl orange and bactericidal activity of Ag doped ZnO nanoparticles. *J. Indian Chem. Soc.* **100**(2), 100920 (2023)
- Sivakumar, S., Robinson, Y., Mala, N.A.: Studies on photocatalytic performance and supercapacitor applications of undoped and Cu-doped ZnO nanoparticles. *J. Appl. Surface Sci. Adv.* **12**, 100344 (2022)
- Gao, Q., Dai, Y., Li, X., Yang, L., Cui, C., Li, C.: Effects of Mn dopant on tuning carrier concentration in Mn doped ZnO nanoparticles synthesized by co-precipitation technique. *J. Mater. Sci.: Mater. Electron.* **29**, 3568–3575 (2018)
- Bordbar, M., Jafari, S., Yeganeh-Faal, A., Khodadadi, B.: Influence of different precursors and Mn doping concentrations on the structural, optical properties and photocatalytic activity of single-crystal manganese-doped ZnO. *J. Iran. Chem. Soc.* **14**, 897–906 (2017)
- Guo, S., Hou, Q., Zhao, C., Zhang, Y.: Study of the effect of Cu heavy doping on band gap and absorption spectrum of ZnO. *Chem. Phys. Lett.* **614**, 15–20 (2014)
- Abed, S., Bougharraf, H., Bouchouit, K., Sofiani, Z., Derkowska-Zielinska, B., Aida, M., Sahraoui, B.: Microstructures, Influence of Bi doping on the electrical and optical properties of ZnO thin films. *J. Superlattices* **85**, 370–378 (2015)
- Akcan, D., Gungor, A., Arda, L.: Structural and optical properties of Na-doped ZnO films. *J. Mol. Struct.* **1161**, 299–305 (2018)
- Poongodi, G., Anandan, P., Kumar, R.M., Jayavel, R.: Studies on visible light photocatalytic and antibacterial activities of nanostructured cobalt doped ZnO thin films prepared by sol-gel spin coating method. *Spectrochim. Acta Part A Mol. Biomol. Spectrosc.* **148**, 237–243 (2015)
- Hsiou, Y.-F., Hung, W.-K., Wang, C.-W.: Fabrication of Sb-doped p-type ZnO thin films by pulsed laser deposition. *Atlas J. Mater. Sci.* **2**(1), 60–64 (2015)
- Ootsuka, T., Liu, Z., Osamura, M., Fukuzawa, Y., Kuroda, R., Suzuki, Y., Otagawa, N., Mise, T., Wang, S., Hoshino, Y.: Studies on aluminum-doped ZnO films for transparent electrode and antireflection coating of β -FeSi₂ optoelectronic devices. *Thin Solid Films* **476**(1), 30–34 (2005)
- Karyaoui, M., Mhamdi, A., Kaouach, H., Labidi, A., Boukha-chem, A., Boubaker, K., Amlouk, M., Chtourou, R.: Some physical investigations on silver-doped ZnO sprayed thin films. *Mater. Sci. Semicond. Process.* **30**, 255–262 (2015)
- Boukhari, A., Deghfel, B., Mahroug, A., Amari, R., Selmi, N., Kheawhom, S., Mohamad, A.A.: Thickness effect on the properties of Mn-doped ZnO thin films synthesis by sol-gel and comparison to first-principles calculations. *Ceram. Int.* **47**(12), 17276–17285 (2021)
- Mahroug, A., Amari, R., Boukhari, A., Deghfel, B., Guerbous, L., Selmi, N.: Synthesis, structural, morphological, electronic, optical and luminescence properties of pure and manganese-doped zinc oxide nanostructured thin films: effect of doping. *J. Nanoelectron. Optoelectron.* **13**(5), 732–742 (2018)
- Benrezgaa, E., Deghfel, B., Abdelhalim, Z., Basirun, W. J., Amari, R., Boukhari, A., Yaakob, M.K., Kheawhom, S., Mohamad, A.A.: Synthesis and properties of copper doped zinc oxide thin films by sol-gel, spin coating and dipping: a characterization review. *J. Mol. Struct.* **1267**, 133639 (2022)

21. Boukhari, A., Deghfel, B., Mahroug, A., Amari, R., Selmi, N., Mohamad, A.A.: In Thickness effect on the properties of 4% Mn-doped ZnO thin films grown by sol-gel spin coating deposition. *Macromolecular Symposia*. **397**(1), 2000235 (2021)
22. Borah, D., Baruah, M.K., Saikia, P.P., Senapoty, K.K., Barua, M., Singha, R.: Structural characterization and surface environment of ZnO nanoflowers. *J. Mater. Environ. Sci.* **7**, 310–315 (2016)
23. Yin, H., Casey, P.S.: ZnO nanorod composite with quenched photoactivity for UV protection application. *Mater. Lett.* **121**, 8–11 (2014)
24. Jagadish, C., Pearton, S.J.: Zinc oxide bulk, thin films and nanostructures: processing, properties, and applications. Elsevier (2011)
25. Narayanan, N., Deepak, N.K.: Enhancement of visible luminescence and photocatalytic activity of ZnO thin films via Cu doping. *Optik* **158**, 1313–1326 (2018)
26. Geldasa, F.T., Kebede, M.A., Shura, M.W., Hone, F.G.: Experimental and computational study of metal oxide nanoparticles for the photocatalytic degradation of organic pollutants: a review. *RSC Adv.* **13**(27), 18404–18442 (2023)
27. Amari, R., Benrezgaa, E., Deghfel, B., Abdelhalim, Z., Yaakob, M.K., Basirun, W.J., Boukhari, A., Kheawhom, S., Mohamad, A.A.: Ni doping effect on the electronic, structural and optical properties of ZnO nanoparticles prepared by Co-precipitation route. *J. Opt. Mater.* **128**, 112398 (2022)
28. Dhivya, A., Yadav, R.: An Eco-approach synthesis of undoped and Mn doped ZnO nano-photocatalyst for prompt decoloration of methylene blue dye. *J. Mater. Today: Proc.* **48**, 494–501 (2022)
29. Rajagopal, S., Paramasivam, B., Muniyasamy, K.: Photocatalytic removal of cationic and anionic dyes in the textile wastewater by H₂O₂ assisted TiO₂ and micro-cellulose composites. *J. Separ. Purif. Technol.* **252**, 117444 (2020)
30. Shanmugam, P., Ngullie, R.C., Smith, S.M., Boonyuen, S., Boddula, R., Pothu, R.: Visible-light induced photocatalytic removal of methylene blue dye by copper oxide decorated zinc oxide nanorods. *J. Mater. Sci. Energy Technol.* **6**, 359–367 (2023)
31. Singh, R., Barman, P., Sharma, D.: Synthesis, structural and optical properties of Ag doped ZnO nanoparticles with enhanced photocatalytic properties by photo degradation of organic dyes. *J. Mater. Sci.: Mater. Electron.* **28**, 5705–5717 (2017)
32. Pham, A.T.T., Van Hoang, D., Nguyen, T.H., Le, O.K.T., Wong, D.P., Kuo, J.-L., Chen, K.-H., Phan, T.B., Tran, V.C.: Compounds, Hydrogen enhancing Ga doping efficiency and electron mobility in high-performance transparent conducting Ga-doped ZnO films. *J. Alloys* **860**, 158518 (2021)
33. Zhu, B., Xie, M., Wang, J., Shi, X., Wu, J., Zeng, D., Xie, C.: Comparative study on effects of H₂ flux on structure and properties of Al-doped ZnO films by RF sputtering in Ar+ H₂ ambient at two substrate temperatures. *J. Ceram Int.* **40**(8), 12093–12104 (2014)
34. Ebrahimi, R., Hossienzadeh, K., Maleki, A., Ghanbari, R., Rezaee, R., Safari, M., Shahmoradi, B., Daraei, H., Jafari, A., Yetilmезsoy, K., Puttaiah, S.H.: Effects of doping zinc oxide nanoparticles with transition metals (Ag, Cu, Mn) on photocatalytic degradation of Direct Blue 15 dye under UV and visible light irradiation. *J. Environ. Health Sci. Eng.* **17**, 479–92 (2019)
35. Mahmutoglu, G., Topsakal, A., Altan, E., Kuskonmaz, N., Dagllar, S., Oktar, F.N., Erdemir, G., Kuruca, S.E., Akyol, S., Gunduz, O., Ben-Nissan, B.: Effects of temperature and pH on the synthesis of nanohydroxyapatite powders by chemical precipitation. *J. Aust. Ceram. Soc.* 1–9 (2023)
36. Noukelag, S.K., Razanamahandry, L.C., Ntwampe, S.K., Arendse, C.J., Maaza, M.: Management, Industrial dye removal using bio-synthesized Ag-doped ZnO nanoparticles. *J. Environ. Nanotechnol. Monitor.* **16**, 100463 (2021)
37. Gopinath, V., Priyadarshini, S., Al-Maleki, A., Alagiri, M., Yahya, R., Saravanan, S., Vadivelu, J.: In vitro toxicity, apoptosis and antimicrobial effects of phyto-mediated copper oxide nanoparticles. *J. RSC Adv.* **6**(112), 110986–110995 (2016)
38. Benrezgaa, E., Deghfel, B., Mahroug, A., Yaakob, M.K., Boukhari, A., Amari, R., Kheawhom, S., Mohamad, A.A.: Experimental and theoretical studies on structural, morphological, electronic, optical and magnetic properties of Zn_{1-x}Cu_xO thin films (0 ≤ x ≤ 0.125). *J. Mater. Sci. Semiconduct. Process.* **134**, 106012 (2021)
39. Amari, R., Deghfel, B., Mahroug, A., Mohamad, A.A., Boukhari, A., Selmi, N.: Effects of Mn doping on the structural, morphological, electronic and optical properties of ZnO thin films by sol-gel spin coating method: an experimental and DFT+ U study. *J. Phys. B: Condensed Matter* **577**, 411766 (2020)
40. Samavati, A., Ismail, A., Nur, H., Othaman, Z., Mustafa, M.: Spectral features and antibacterial properties of Cu-doped ZnO nanoparticles prepared by sol-gel method. *J. Chin. Phys. B* **25**(7), 077803 (2016)
41. Naik, E.I., Naik, H.B., Swamy, B.K., Viswanath, R., Gowda, I.S., Prabhakara, M., Chetankumar, K.: Influence of Cu doping on ZnO nanoparticles for improved structural, optical, electrochemical properties and their applications in efficient detection of latent fingerprints. *J. Chem. Data Collect.* **33**, 100671 (2021)
42. Szczesny, R., Scigala, A., Derkowska-Zielinska, B., Skowronski, L., Cassagne, C., Boudebs, G., Viter, R., Szlyk, E.: Synthesis, optical, and morphological studies of zno powders and thin films fabricated by wet chemical methods. *J. Mater.* **13**(11), 2559 (2020)
43. Rafique, S., Kasi, A.K., Kasi, J.K., Aminullah, Bokhari, M., Shakoor, Z.: Nanotechnology, Fabrication of silver-doped zinc oxide nanorods piezoelectric nanogenerator on cotton fabric to utilize and optimize the charging system. *J. Nanomat.* **10**, 1847980419895741 (2020)
44. Yayapao, O., Thongtem, T., Phuruangrat, A., Thongtem, S.: Ultrasonic-assisted synthesis of Nd-doped ZnO for photocatalysis. *J. Mater. Lett.* **90**, 83–86 (2013)
45. Alonizan, N.: Photoluminescence properties of Al-doped ZnO synthesized via facile sol-gel route. *J. Alloys Compounds* **912**, 165084 (2022)
46. Guruvammal, D., Selvaraj, S., Sundar, S.M.: Structural, optical and magnetic properties of Co doped ZnO DMS nanoparticles by microwave irradiation method. *J. Magn. Magn. Mater.* **452**, 335–342 (2018)
47. Ray, P.G., Das, M., Wan, M., Jacob, C., Roy, S., Basak, P., Dhara, S.: Surfactant and catalyst free facile synthesis of Al-doped ZnO nanorods—an approach towards fabrication of single nanorod electrical devices. *J. Appl. Surf. Sci.* **512**, 145732 (2020)
48. Mallika, A., RamachandraReddy, A., SowriBabu, K., Reddy, K.V.: Synthesis and optical characterization of aluminum doped ZnO nanoparticles. *Ceram. Int.* **40**(8), 12171–12177 (2014)
49. Steffy, K., Shanthi, G., Maroky, A.S., Selvakumar, S.: Synthesis and characterization of ZnO phytonanocomposite using *Strychnos nux-vomica* L.(Loganiaceae) and antimicrobial activity against multidrug-resistant bacterial strains from diabetic foot ulcer. *J. Adv. Res.* **9**, 69–77 (2018)
50. Purwaningsih, S., Pratapa, S., Triwikantoro, D.: In Nano-sized ZnO powders prepared by co-precipitation method with various pH. *AIP Confer Proc.* **1752**(1), 020063 (2016)
51. Raskar, N., Dake, D., Khawal, H., Deshpande, U., Asokan, K., Dole, B.: Development of oxygen vacancies and surface defects in Mn-doped ZnO nanoflowers for enhancing visible light photocatalytic activity. *J. SN Appl. Sci.* **2**, 1–11 (2020)
52. George, N.S., Kadam, S.A., Sreehari, S., Jose, L.M., Ma, Y.-R., Aravind, A.: Inquest on photocatalytic and antibacterial traits of low composition Cu doped ZnO nanoparticles. *J. Chem. Phys. Lett.* **815**, 140351 (2023)
53. Hosseini, S., Sarsari, I.A., Kameli, P., Salamati, H.: Compounds, Effect of Ag doping on structural, optical, and photocatalytic properties of ZnO nanoparticles. *J. Alloys* **640**, 408–415 (2015)

54. Mahdavi, R., Talesh, S.S.A.: Sol-gel synthesis, structural and enhanced photocatalytic performance of Al doped ZnO nanoparticles. *Adv. Powder Technol.* **28**(5), 1418–1425 (2017)
55. Guo, Y., Fu, X., Xie, Y., Zhu, L., Liu, R., Liu, L.: Synthesis of Ag/ZnO nanocomposites with enhanced visible photocatalytic performance. *Opt. Mater.* **133**, 112980 (2022)
56. Ong, C.B., Ng, L.Y., Mohammad, A.W.: A review of ZnO nanoparticles as solar photocatalysts: synthesis, mechanisms and applications. *Renew. Sustain. Energy Rev.* **81**, 536–551 (2018)

Publisher's Note Springer Nature remains neutral with regard to jurisdictional claims in published maps and institutional affiliations.

Springer Nature or its licensor (e.g. a society or other partner) holds exclusive rights to this article under a publishing agreement with the author(s) or other rightsholder(s); author self-archiving of the accepted manuscript version of this article is solely governed by the terms of such publishing agreement and applicable law.